Negative ions in a radio-frequency oxygen plasma

E. Stoffels, W.W. Stoffels, D. Vender, M. Kando,* G.M.W. Kroesen, and F.J. de Hoog
Department of Physics, Eindhoven University of Technology, P.O. Box 513, 5600 MB Eindhoven, The Netherlands
(Received 5 July 1994)

A systematic study of a low pressure (5–200 mTorr) oxygen discharge is presented. Measurements of the electron and negative ion densities in the 13.56 MHz capacitively coupled plasma are performed by means of a microwave resonance technique in combination with photodetachment. A kinetic model is developed, incorporating volume and wall reactions of ions as well as neutral species. It is shown, by matching the experimental results with the model, that the dominant ion is O^- whereas the O_2^- and O_3^- densities reach 10 to 20 % of the total negative ion density. The ratio of negative ion to electron density varies between 5 and 10 and decreases with pressure and rf power. The total negative ion density is about 5×10^{15} m^{-3}, it increases with gas flow, is independent of the rf input power, and has a maximum at a pressure of 30 mTorr. The agreement between the measurements and the model is within the experimental error for a wide range of conditions. Deviations are explained by changes in the gas and wall temperatures. From the known ion density the effective ionization rate has been determined and related to the electron temperature. The ionization temperature obtained in this way varies between 2 and 4 eV and decreases with increasing gas pressure and power, as expected for the bulk electron temperature in this type of discharge.

PACS number(s): 52.80.Pi, 82.20.−w, 82.40.Ra, 52.40.Hf

I. INTRODUCTION

Oxygen plasmas are widely used for industrial materials processing, due to their ability to clean, oxidize, etch, and ash samples without heating them to high temperatures [1–5]. Applications include dry etching of photoresist, polymer, and biological materials, formation of oxide films, and ashing for pretreatment of specimens in chemical analysis. Furthermore, some oxygen discharges are efficient sources of ozone, atomic oxygen, and a variety of excited species [6].

In this work a low pressure radio-frequency (rf) oxygen discharge is treated. The relative simplicity of oxygen in comparison to other etchants (such as CF_4 and SF_6) and the presence of a wide database of reaction constants makes the O_2 discharge a good modeling subject. This leads to insight into important physical plasma processes and possibly to the extension of some of the conclusions to chemically more complicated systems. However, even in a relatively simple oxygen discharge a wide variety of species can be formed in the gas phase as well as at bounding surfaces, which makes the chemistry of this plasma still sufficiently complex to warrant detailed investigation. Only a combined experimental and theoretical study can remove some of the uncertainties in the relative importance of various processes and how they influence the discharge behavior. In such a study particular attention must be paid to the behavior of the charged species since they determine both physical and chemical features of the plasma, such as the rf power dissipation, the structure of the plasma sheath, and the fluxes of reactive molecules reaching the surface. As O_2 is an electronegative gas, negative ions (O^-, O_2^-, and O_3^-) are expected to contribute significantly to the total charge balance in an oxygen plasma.

In the past both experimental [7,8] and theoretical studies [9,10] were devoted mainly to oxygen plasmas at pressures above 500 mTorr. However, low pressure discharges for surface modification are now also attracting attention [11–13]. Here we present measurements of the absolute densities of charged particles in such a discharge. Previous measurements have been performed using probe and optogalvanic methods by Yasuda *et al.* [14]. In the present study a microwave resonance method is combined with laser induced photodetachment in order to obtain electron and total negative ion densities. Moreover, the O_2^- density is obtained by performing selective photodetachment of the O_2^- ion. A kinetic model is used to clarify the implications of the measurements and it follows that O^- is the dominant negative ion. However, a significant fraction (about 10%) of O_2^- and O_3^- can also be present in the plasma, which agrees with the data of Suzuki and Kasuya [15]. The dependencies of the total ion density and the O_2^- density on various plasma parameters have been measured and elucidated in terms of elementary plasma processes. The experimental dependencies help to estimate the rates of some (mainly heterogeneous) processes, which are either not reported or subject to discussion in literature.

II. EXPERIMENT

A. Plasma reactor

The measurements have been carried out in a 13.56 MHz capacitively coupled plasma confined in an

*Permanent address: Department of Chemical Engineering, Shizuoka University, Johoku 3-5-1, Hamamatsu 432, Japan.

aluminum cylinder with a diameter of 17.5 cm and a height of 5 cm, as shown in Fig. 1. The lower rf electrode is water cooled and has a diameter of 12 cm. The discharge is sustained by an ENI rf generator combined with an automatic matching network to optimize the power dissipation in the plasma. The input power can be varied between 0 and 120 W. Feed gases pass through mass flow controllers and are introduced homogeneously through a slit around the rf electrode. The pressure in the plasma is measured using a mks baratron. The gas pressure and flow can be varied independently, from 5 to 500 mTorr and from 0 to 100 SCCM (SCCM denotes cubic centimeter per minute at STP), respectively, using a throttle valve in the pumping line of a turbo molecular pump.

B. Microwave resonance and photodetachment

In order to measure the electron density a microwave resonance method has been used in which the cylinder containing the plasma serves as a cavity. For this purpose a low power microwave signal of variable frequency is coupled into the plasma cavity by means of an antenna, exciting the TM_{020} mode (frequency $\sim$ 3 GHz). The transmission of the cavity is recorded by another antenna and processed by a digitizing oscilloscope. The resonance frequency of the cavity, which depends on the number of free electrons within, is determined by tuning the microwave frequency to maximum transmission. From the shift of the resonance frequency ($\Delta f = f - f_0$) with respect to its value in vacuum (f_0) the microwave field averaged electron density (n_{e0}) is deduced [16,17]:

$$n_{e0} = \frac{2\,\Delta f\, m_e \epsilon_0 (2\pi f)^2}{f_0 e^2}, \tag{1}$$

with ϵ_0 the vacuum electric permittivity, and m_e and e, respectively, the electronic mass and charge. This method does not provide any spatial resolution as n_{e0} is merely a space ($\vec{x}$) averaged density weighted with the square of the field strength (E^2),

$$n_{e0} = \frac{\int_{\text{cavity}} n_e(\vec{x}) E(\vec{x})^2 d\vec{x}}{\int_{\text{cavity}} E(\vec{x})^2 d\vec{x}}. \tag{2}$$

An assumption must therefore be made about the spatial distribution of the electrons in order to obtain a more useful value of the electron density. A first simplification follows from the cylindrical symmetry of the electron density and E. Further, the applied TM_{020} mode has only an axial field component given by a Bessel function $J_0(r)$ with only radial dependence. Models of electronegative plasmas have shown that the electron density is flat in the whole plasma glow and a sharp decrease is found in the space charge region towards the electrodes [18,19]. The same conclusion follows from optical emission measurements [20]. As the diameter of the cavity is large in comparison to the thin sheath at the grounded sidewall ($\leq$ 5 mm), the radial dependence of the electron density can be neglected. However, the axial profile can be important since the large sheath at the powered electrode (up to 2 cm) is not much smaller than the height of the cavity (H = 5 cm). We therefore measure the axial thickness of the plasma glow for every plasma condition, using the negative ion density profiles (see below), and multiply the density from Eq. (1) (i.e., averaged over the cavity volume) by the ratio of the height of the cavity to the glow thickness, thus obtaining an average electron density in the plasma glow. As the field averaged electron density can be determined very accurately (to better than 0.1%), the main uncertainty resulting from using the microwave method is caused by a limited knowledge of the electron density profile. This uncertainty results in an estimated error of about 10% in the average electron density.

The microwave resonance method can be modified to obtain the negative ion density as well. A Nd:YAG (YAG denotes yttrium aluminum garnet) laser is used to photodetach electrons from the negative ions and the additional shift in the resonance frequency, caused by the detached electrons, is measured. Applying Eq. (1) to this extra frequency shift gives the field averaged density of the detached electrons Δn_e. At sufficiently high laser power, the photodetachment signal saturates and the radially averaged negative ion density n_- is obtained by multiplying Δn_e by the ratio of the cavity and the laser beam volume, weighted with E^2:

$$n_- = \Delta n_e \frac{S \int_{-R}^{R} E(r)^2 dr}{\int_{\text{cavity}} E(\vec{x})^2 d\vec{x}}, \tag{3}$$

with R the radius of the cavity and S the cross section of the laser beam.

Although the laser beam radius is controlled by a diaphragm, the uncertainty in the beam radius imposes an error of about 20% on the measured negative ion density. The laser beam passes through two vertical slits in the plasma cavity allowing for axial scans. The spatial resolution is determined by the laser beam diameter, which in our case is 2 mm. Since the negative ions are present only in the plasma glow, their profiles can be used to determine the glow thickness, needed for the correction of the electron density, as explained above. The photodetachment technique allows determination of the densities of various negative ions in the plasma through selective detection of different species according to their detachment energies (electron affinities) by choosing an appropriate

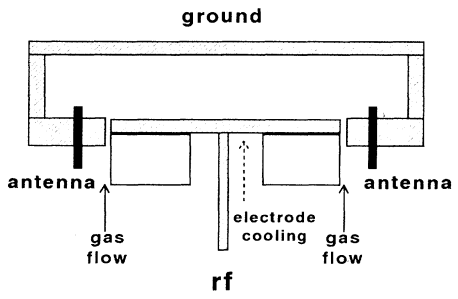

FIG. 1. The cylindrical plasma chamber which simultaneously serves as a microwave cavity.

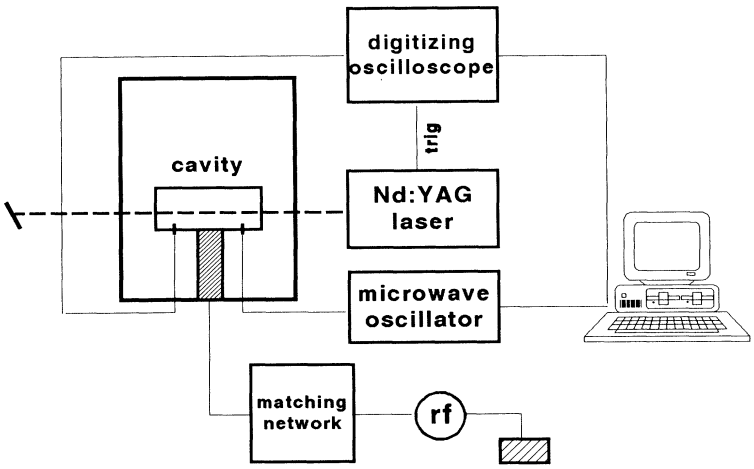

FIG. 2. Experimental setup for negative ion density measurements.

laser photon energy, e.g., by using a dye laser. In the case of an oxygen plasma the most important ions are O^-, $O_2{}^-$, and $O_3{}^-$, with detachment energies 1.46 eV, 0.44 eV, and 2.10 eV, respectively [21,22]. Using the frequency doubled beam (λ = 532 nm, 2.3 eV) we determine the total negative ion density. In addition, by using the fundamental frequency of the Nd:YAG laser (λ = 1064 nm, 1.16 eV) it is possible to separate $O_2{}^-$ from the other ions. As the abundance of $O_2{}^-$ in the plasma is low, we expand the infrared beam to 3.5 mm diameter in order to achieve a higher sensitivity in this case.

A sketch of the complete experimental setup for the density measurements is shown in Fig. 2. For a typical measurement the personal computer (PC) prepares the settings of the microwave oscillator and the oscilloscope. Then the laser is fired, which triggers the oscilloscope to measure the time dependent microwave transmission signal and store the data on the PC. This procedure is repeated until the resonance curve of the cavity is scanned. Finally the PC calculates the time dependent electron density from the stored data. The vacuum vessel is moved by stepper motors to obtain the axial negative ion density profiles.

III. KINETIC MODEL

A global kinetic model of the discharge has been developed in order to explain the experimentally observed negative ion densities. The model facilitates comparisons of the importance of several elementary processes involving negative ions, such as ion-ion recombination and associative detachment. Table I gives an overview of the reactions incorporated into the model. Since three body collisions are only important at pressures above 1 Torr, they have been neglected. Furthermore, the low gas temperature in a low pressure rf discharge ($\approx$ 300 K) allows us to neglect reactions requiring highly energetic heavy particles. The highly energetic heavy particles in the sheath can have an influence on the bulk chemistry only at very low pressures ($\leq$ 20 mTorr). It will be shown in Sec. IV C that the negative ion density at these pressures does not depend on the plasma chemistry. Therefore threshold processes such as excitation (reaction 3), dissociation (1,2,5), and ionization are assumed to be electron induced only. The negative ions are formed by dissociative attachment (6,7,13) or by charge transfer (12,16,18,20). They are destroyed by ion-ion neutralization (8,14,19), neutral detachment (10,15,17,21), and electron detachment (11). The neutral species are lost by diffusion to the wall (22,24) and by gas flow (25). It is clear that these heterogeneous processes result in density gradients in the plasma. The error due to introducing space independent (average) densities into the rate equations (i.e., $\langle n_1\rangle\langle n_2\rangle$ instead of $\langle n_1 n_2\rangle$) can be estimated from the predicted density profiles. As all profiles are expected to be either flat or close to parabolic (see Appendix), this error is less than 20%.

The input parameters for the calculations are pressure, gas flow, and the experimentally determined electron density. As the latter changes with the input power, a complete set of experimental variables (pressure, gas flow, and power input) is introduced into the model. The following species are taken into account: ground state O_2 ($X\,{}^3\Sigma_g^-$), the metastable $O_2(a)$ ($a^1\Delta_g$, $E_{\rm exc}$ = 0.99 eV), ground state O, O_3, O^-, $O_2{}^-$, and $O_3{}^-$. The reaction rates of $O_2(b)$ ($b\,{}^1\Sigma_g^+$, $E_{\rm exc}$ = 1.6 eV) are not significantly higher than those of $O_2(a)$, while its density does not exceed 20% of the $O_2(a)$ density. As the effect of $O_2(b)$ on negative ion densities is of the order of the accuracy of the rate constants, this species has been neglected here. For the same reason excited atomic oxygen states are not incorporated in the model. The listed rates in Table I are based on literature values. The rates of electron induced processes are complicated functions of the electron temperature (T_e). For clarity, only their numerical values at T_e = 3 eV are listed in Table 1. The diffusion loss frequency of neutral species (22,24) is estimated using an effective gradient length $\Lambda_{\rm eff}$ (see Appendix), in which geometrical factors as well as the sticking coefficient γ are included. The flow loss frequency for neutral species (25) is given by

$$\nu_{25} = \frac{760 \times 10^{-6} \mathcal{F}}{60 V_{\rm pl} p} \quad (4)$$

where the flow $\mathcal{F}$ is in SCCM, the pressure p is in Torr, and the plasma volume $V_{\rm pl} = 1.2 \times 10^{-3}$ m^3.

Some of the rate constants (10,12) used in the calculations are modified and estimates are made for sticking coefficients of various species. This is treated in detail in Sec. IV B. The stationary state balance equations, containing all processes from Table I, are solved analytically using the elimination method. The balance equation for O_2 is replaced by the particle balance: $O_2 + O_2(a) + O + O_3$ equals the total neutral density known from the pressure.

An important issue in all models is the electron energy distribution function (EEDF). As there is no direct experimental evidence of both the average electron energy and the shape of the distribution function in our discharge, we assume a Maxwellian distribution for the bulk electrons, with a temperature $T_e = 3$ eV. Similar values in rf discharges have been found by several investigators [23,24]. However, it will be shown in Sec. IV C that the negative ion density does not strongly depend on the electron temperature.

In our model the positive ion density is obtained from the charge neutrality condition and not from the positive ion balance equation. The dominant positive ion in this low pressure O_2 rf plasma is O_2^+, as found from mass spectrometry measurements performed on a separate but geometrically similar apparatus, which has been described by Snijkers *et al.* [25]. For the whole range of conditions dealt with in this study, O^+ made up less than 10% of the escaping ion flux. The positive ion density n_+ is determined by the ionization rate ($k_{\rm ion}$) and by the wall loss and recombination rate $k_{\rm rec} = 1 \times 10^{-13}$ m^3 s^{-1} with negative ions n_-:

$$k_{\rm ion} n_e \{[O_2] + [O_2(a)] \exp(0.99/T_e)\} = \frac{D_a}{\Lambda_{\rm eff}^2} n_+ + k_{\rm rec} n_+ n_- . \quad (5)$$

TABLE I. Overview of the reactions in the kinetic model, with the rate constants for $T_e = 3$ eV, $T_g = 300$ K. D denotes the diffusion coefficient, in m^{2}s^{-1}, $\Lambda_{\rm eff}$ denotes the effective diffusion length from Eq. (A9), and γ the sticking probability. The pressure p is in Torr and the flow $\mathcal{F}$ in SCCM.

Reaction[a]				Rate constant (m^3 s^{-1}) or frequency (s^{-1})[b]	Reference
Neutral species:					
(1)	$O_2 + e$	$\rightarrow$	$2O + e$	2.4×10^{-15}	[9]
(2)	$O_2(a) + e$	$\rightarrow$	$2O + e$	$k_1 \exp(0.99/T_e)$	estimate
(3)	$O_2 + e$	$\rightarrow$	$O_2(a) + e$	6.1×10^{-16}	[26]
(4)	$O_2(a) + e$	$\rightarrow$	$O_2 + e$	$(3/2) k_3 \exp(0.99/T_e)$	detailed balance
(5)	$O_3 + e$	$\rightarrow$	$O + O_2 + e$	$5k_1$	[27]
O^-:					
(6)	$O_2 + e$	$\rightarrow$	$O^- + O$	3.5×10^{-17}	[26]
(7)	$O_2(a) + e$	$\rightarrow$	$O^- + O$	1.2×10^{-16}	[26]
(8)	$O^- + O_2^+$	$\rightarrow$	neutrals	10^{-13}	[28]
(9)	$O^- + O$	$\rightarrow$	$O_2 + e$	1.4×10^{-16}	[29]
(10)	$O^- + O_2(a)$	$\rightarrow$	$O_3 + e$	10^{-16}	[10], see text
(11)	$O^- + e$	$\rightarrow$	$O + 2e$	2.4×10^{-14}	[30]
O_2^-:					
(12)	$O^- + O_2(a)$	$\rightarrow$	$O + O_2^-$	3.3×10^{-17}	[10], see text
(13)	$O_3 + e$	$\rightarrow$	$O_2^- + O$	10^{-15}	[10]
(14)	$O_2^- + O_2^+$	$\rightarrow$	neutrals	10^{-13}	[28]
(15)	$O_2^- + O$	$\rightarrow$	$O_3 + e$	1.5×10^{-16}	[10]
(16)	$O_2^- + O$	$\rightarrow$	$O_2 + O^-$	3.3×10^{-16}	[10]
(17)	$O_2^- + O_2(a)$	$\rightarrow$	$2O_2 + e$	2×10^{-16}	[10]
O_3^-:					
(18)	$O^- + O_3$	$\rightarrow$	$O + O_3^-$	5.6×10^{-16}	[10]
(19)	$O_3^- + O_2^+$	$\rightarrow$	neutrals	10^{-13}	[28]
(20)	$O_3^- + O$	$\rightarrow$	$O_2^- + O_2$	3.2×10^{-16}	[10]
(21)	$O_3^- + O$	$\rightarrow$	$2O_2 + e$	3×10^{-16}	[10]
Wall processes:				$\nu = D/\Lambda_{\rm eff}^2$	see Appendix
(22)	$O + O_{\rm wall}$	$\rightarrow$	O_2	$D = 2.05 \times 10^{-2} p^{-1}, \gamma = 0.5$	[9,31]
(23)	$O + O_{\rm wall}$	$\rightarrow$	$O_2(a)$	$\nu_{22} \times 3/(10 + \mathcal{F}^2)$	see text
(24)	$O_2(a)$	$\rightarrow$	O_2	$\gamma = 0$	[32], see text
Flow loss:					
(25)	for O, $O_2(a)$, O_3			$0.01 \mathcal{F}/p$	

[a]The reactions are referred to in the text by giving their number from the table enclosed in parentheses.

[b]Numbered subscripts refer to the relevant reaction number.

This balance contains the ionization of O_2 and $O_2(a)$. The latter has been corrected for the excitation energy, as in the case of dissociation (1,2), but it remains a minor contribution. The dominant loss process is ambipolar diffusion to the wall. The ambipolar diffusion coefficient D_a in the presence of negative ions is related to the ordinary thermal diffusion coefficient ($D_{\rm th}$) by [19]

$$D_a \approx D_{\rm th}\frac{1+(T_e/T_i)[1+2(n_-/n_e)]}{1+(T_e/T_i)(n_-/n_e)}, \qquad (6)$$

where T_i is the ion temperature. Assuming $T_e/T_i \gg 1$ this reduces to $D_a \approx (2+n_e/n_-)D_{\rm th}$. The value of $D_{\rm th}$ is $6\times10^{-3}/p\,{\rm m}^2/{\rm s}$, where p is in Torr [9]. The gradient length for ions is taken as $\Lambda_{\rm eff} = H_g/\sqrt{12}$ (see Appendix), where H_g is the experimentally determined glow thickness.

The charge neutrality condition together with the positive ion balance determine the electron temperature in the plasma. In Eq. (5) only the ionization rate is strongly temperature dependent so substituting known ion densities into Eq. (5) gives the ionization rate and consequently the electron temperature (see Secs. IV C and IV D). As mentioned previously, this assumes a Maxwellian electron velocity distribution.

IV. RESULTS AND DISCUSSION

A. Electron density

The measured electron density as a function of power and pressure is shown in Figs. 3 and 4. The electron density rises almost linearly with the input power which is not corrected for the power losses in the matching network. These losses may account for up to 20% of the nominal power level. The electron density rises sharply with increasing pressure up to about 50 mTorr with a broad maximum around 60 mTorr and a slight decrease at higher pressures. There is no measurable gas flow dependence of the electron density. The electron density data, fitted by an empirical expression, are used as an input parameter for the calculations. The dependencies of the total negative ion density and the O_2^- density on the gas flow, the pressure, and the rf power are discussed in the following three sections.

B. Gas flow dependence

The flow dependence of the negative ion densities is compared to the model in Fig. 5 for a pressure of 25 mTorr and in Fig. 6 for 100 mTorr. There is good agreement between the model and the measurements at 25 mTorr except at the very lowest flow. The agreement is somewhat less satisfactory at 100 mTorr, with the discrepancy occurring again at low flow. Possible causes of this are discussed below.

Varying the residence time of the neutral species in the discharge volume is very important in studying the plasma since it allows us to separately investigate purely chemical effects such as a changing gas composition.

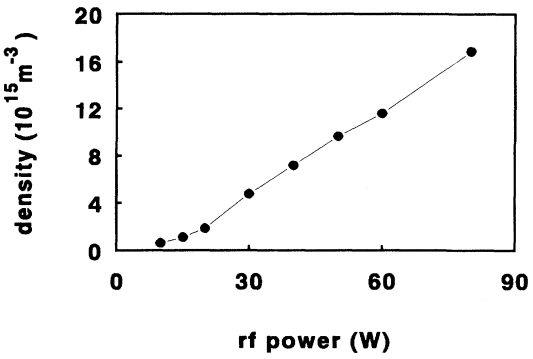

FIG. 3. Electron density as a function of the rf input power. The pressure is 30 mTorr and the gas flow is 30 SCCM. SCCM denotes cubic centimeter per minute at STP.

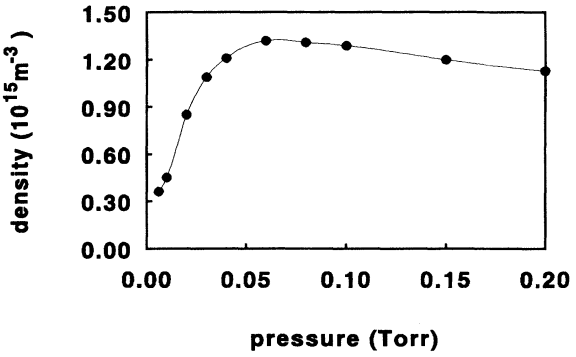

FIG. 4. Electron density as a function of pressure. Input power is 10 W, flow is 30 SCCM. The line indicates the parametric fit which has been used as input for the calculations.

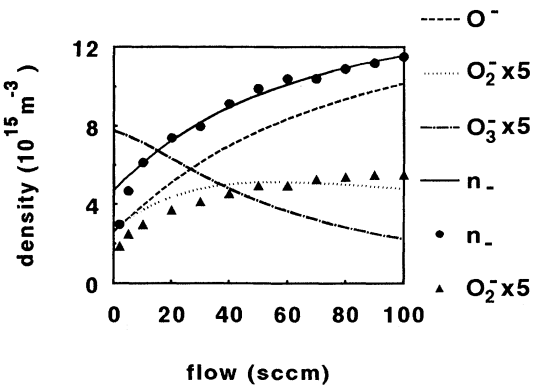

FIG. 5. Measured and calculated negative ion densities as a function of the gas flow. The pressure is 25 mTorr and the input power is 10 W. The dots and solid line indicate the measured and calculated total negative ion density. The calculated O^- density is denoted by the dashed line. The O_2^- density, denoted by triangles and dotted line, and the O_3^- density (dash-dotted line) are shown enlarged five times. Reaction (23) is not incorporated into the calculations.

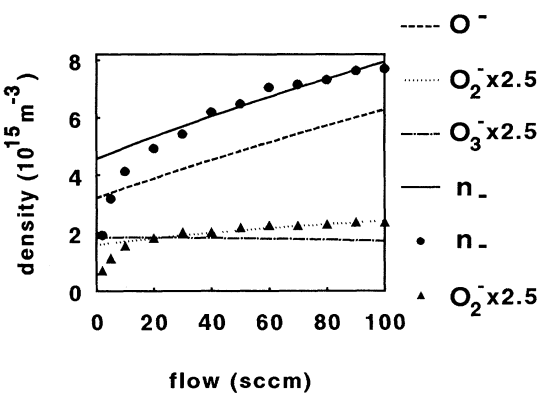

FIG. 6. Measured and calculated ion density as a function of the gas flow. The pressure is 100 mTorr and the input power is 10 W. The symbols are identical with Fig. 5. In this case the O_2^- and O_3^- densities are shown enlarged by a factor 2.5. Reaction (23) is not incorporated into the calculations.

Since the residence time (determined by flow and pressure) is relatively long in comparison to lifetimes of charged particles, only reasonably stable neutral species can contribute to the flow dependence of the negative ion density shown in Figs. 5 and 6. These neutral particles are most likely detaching species, such as O or $O_2(a)$ (reactions 9,10), which are flushed out of the discharge region at high gas flow values. As a result, the detachment frequency will decrease with increasing flow, causing the ion density to rise. However, for these detaching particles destruction at the wall is potentially a more important loss process than the flow (see Table I), unless their sticking coefficients are very low ($\gamma < 10^{-3}$). As the sticking coefficients are poorly known and heavily dependent on wall material and its pretreatment, we will use the experimental flow dependence of the ion density to estimate them for our plasma conditions.

The sticking coefficient γ for atomic oxygen is strongly dependent on the wall material. Booth and Sadeghi [31] reported a very high value $\gamma \sim 0.5$ on stainless steel, while γ on dielectrics is found to be $10^{-5} - 10^{-3}$ [33]. For our conditions (aluminum walls) it can be expected that the reaction probability is closer to the one given by Booth. Consequently, the O density is not expected to be strongly flow dependent. In addition, we have measured the optical emission intensity of the $3p\,^5P$–$3s\,^5S^0$ O transition at 777 nm as a function of flow. For the upper state, direct electronic excitation from the ground state is the dominant population mechanism. As the electron temperature is not expected to change significantly with flow, this intensity is thus a reasonable measure for the ground state O density. As the observed line emission stays almost constant we conclude that the O density is hardly flow dependent, and consequently it cannot be responsible for the observed dramatic changes in the negative ion densities. Furthermore, the production of O by electron impact dissociation (1,2) is a very fast process. Therefore a very high dissociation degree ($\sim$ 50%) would be reached if atomic oxygen were destroyed only by flow. This in turn would lead to a very low negative ion density, due to reactions (9,15,21), in contradiction with the measurements.

The $O_2(a)$ molecule is another potentially efficient detaching particle, but since it also produces negative ions (7), its net detaching effect is not as strong as that of O. In contrast to O, its sticking coefficient on aluminum surfaces is very low ($< 10^{-3}$, [32]). Moreover, wall production of this low energy molecular state, e.g., by reaction (23), cannot be excluded. In fact, similar processes have been studied in a H_2 discharge, where the reactor wall can be an effective source of the vibrationally excited $H_2(\nu)$ [34]. We have initially assumed that $O_2(a)$ is neither lost nor produced at the wall. Based on these assumptions the densities of neutral particles [O, $O_2(a)$, and O_3] are calculated (see Figs. 7 and 8). These densities and the density ratio of O and $O_2(a)$ agree very well with those measured by Tachibana [11] under similar conditions.

The model yields a flow dependence of the total negative ion density which is similar to the observed one at flows above 20 SCCM. However, the absolute values of n_- are about 2.5 times lower than the measured ones if the rates for recombination (8,14,19) and detachment by $O_2(a)$, given by Kossyi *et al.* [10], are used. Since the ion densities, measured in comparable conditions using probe and optogalvanic methods [14], agree with our data, the discrepancy between the measurements and the model is likely due to uncertain rate constants. Agreement can be obtained by either increasing the production rate for negative ions (6,7) or scaling down their losses in the model. The production rate by dissociative attachment has been measured by a number of investigators and its value is fairly accurately established. The rates of ion-ion recombination and neutral detachment are much more uncertain. The fits shown in Figs. 5 and 6 have been obtained using the recombination rate given by Smirnov [28]. The detachment rates (10,12), given by Kossyi *et al.*, are 3×10^{-16} and 10^{-16} $m^3\,s^{-1}$, respectively. However, Khvorostovskaya and Yankovsky [35] give a lower value for reaction (10) at 400 K. Moreover, they have shown that the detachment rate (10) depends strongly on the gas temperature (T_g) and the ion en-

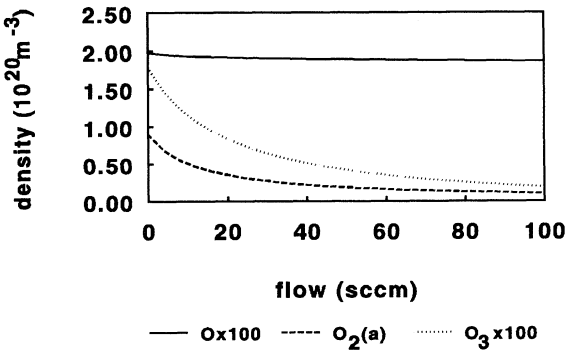

FIG. 7. Calculated densities of $O_2(a)$ (dashed line), O (solid line), and O_3 (dotted line) as a function of gas flow. The pressure is 25 mTorr and the power 10 W. The O and O_3 densities are shown enlarged 100 times.

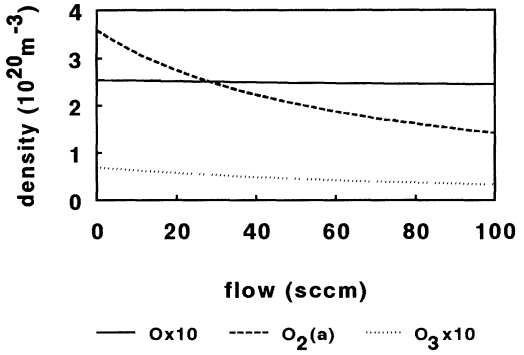

FIG. 8. Calculated densities of $O_2(a)$ (dashed line), O (solid line), and O_3 (dotted line) as a function of gas flow. The pressure is 100 mTorr and the power 10 W. The O and O_3 densities are shown enlarged ten times.

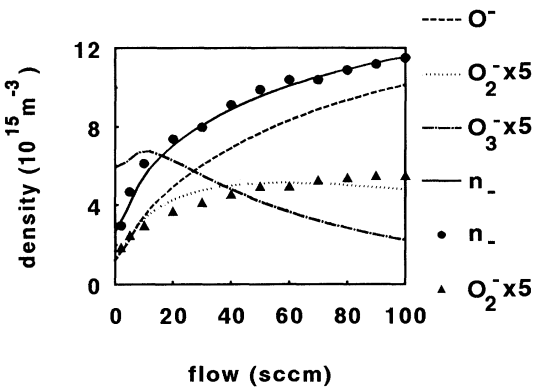

FIG. 9. Measured and calculated negative ion densities as a function of the gas flow. Reaction (23) has been taken into account in the calculations. The conditions are the same as in Fig. 5.

ergy (E_i) as $T_g^{4.0\pm0.4}E_i^{-2.6\pm0.4}$ for $T_g \geq 400$ K. A similar effect can be expected for reaction rate (12). A good agreement between the experiment and the simulation is obtained if we use 10^{-16} m^3 s^{-1} for reaction (10) and 3.3×10^{-17} m^3 s^{-1} for reaction (12).

It can be seen that there is a reasonable agreement between the calculated and the experimental values of n_- and [O_2^-]. However, at low gas flows the calculated values are systematically higher than the measured ones. This discrepancy is especially large at higher pressures (Fig. 6). The rapid decrease of the experimental ion density at low flows indicates an extra loss process, not present in the model. Again it is plausible to assume that this is a detachment process, involving a relatively stable neutral particle, with a stronger density dependence on flow than that of the calculated $O_2(a)$ density. It is unlikely that one of the metastable particles, neglected in the calculations, is responsible for this effect, as, apart from their low densities, any other metastables are expected to have flow dependencies similar to those calculated for $O_2(a)$ or O. A more likely explanation involves an enhancement of $O_2(a)$ or O detachment under the influence of some global parameter such as the wall or gas temperature. In addition to the rates discussed above, heating of the gas and the electrodes at these low flows and higher pressures [36] also changes the surface chemistry, which is expected to be extremely temperature dependent. A possible reaction which would increase the density of detaching species is the wall recombination of atomic oxygen, yielding $O_2(a)$ instead of O_2. A similar process has been described by Sharpless *et al.* [37]. As this is expected to be more efficient at higher temperatures, the heated wall can be an extra source of $O_2(a)$. We cannot determine from our data whether the depletion of negative ions is due to a change of the detachment rates or the $O_2(a)$ density, as both have the same influence on the ion density. We have included this effect in the model by introducing a flow dependent fraction of O, which is converted to $O_2(a)$ at the wall (23). The fitting to the experimental data points shown in Figs. 9 and 10 is obtained when a fraction $3/(10+\mathcal{F}^2)$ (0.03 to 30% for the flows between 100 and 0 SCCM) of the O density lost to the wall returns as $O_2(a)$. This production term has a significant contribution only for low flows ($\leq$ 20 SCCM).

The measured flow dependence of the O_2^- density is very similar to that of O^- (Figs. 5 and 6). Such a dependence can be obtained if O_2^- is produced by charge exchange between $O_2(a)$ and O^- and destroyed by detachment with $O_2(a)$ (17). However, for pressures below 20 mTorr the radical density is lower and ion-ion recombination (14) becomes dominant. In this case the O_2^- density will be proportional to the $O_2(a)$ rather than the O^- density, resulting in a decrease of the O_2^- density with flow for these pressures. A slight influence of recombination can be seen in the calculated data at 25 mTorr in Fig. 9, where the O_2^- density starts to decrease at high gas flows. As this feature is not present in the experimental data, we conclude that the model slightly overestimates the recombination (14) with respect to detachment (15,17).

C. Pressure dependence

The pressure dependencies of the negative ion densities are shown in Figs. 11 and 12. The experimental points

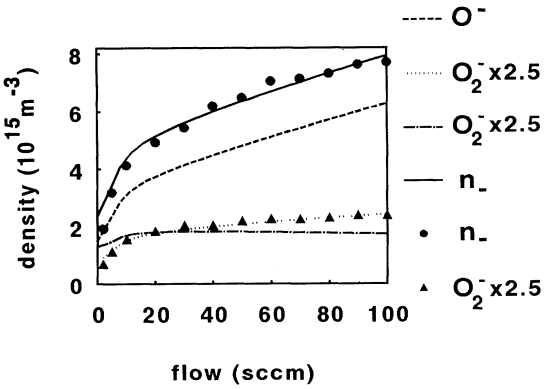

FIG. 10. Measured and calculated negative ion densities as a function of the gas flow. Reaction (23) has been taken into account in the calculations. The conditions are the same as in Fig. 6.

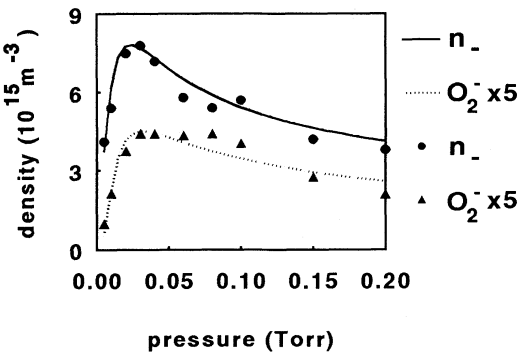

FIG. 11. The measured and calculated total negative ion density (dots and solid line) and the O_2^- density (triangles and dotted line) as a function of pressure. The gas flow is 30 SCCM and the input power 10 W. The experimental densities shown are the averaged values over the plasma glow. The O_2^- density is enlarged five times. The calculations have been performed for $T_e = 3$ eV.

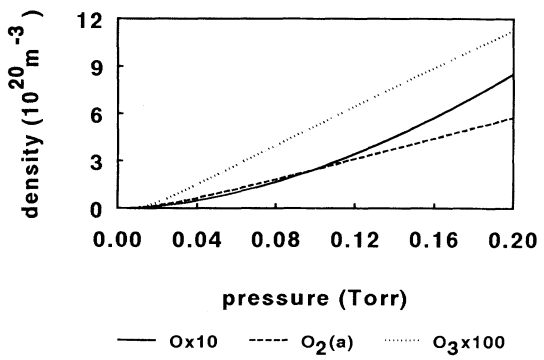

FIG. 13. The calculated neutral densities as a function of pressure at $T_e = 3$ eV, for gas flow 30 SCCM and input power 10 W. The dashed line represents $O_2(a)$, the solid line O, and the dotted line O_3. The densities of O and O_3 are shown multiplied by a factor 10 and 100, respectively.

are the average densities in the plasma glow. The ratio of the total negative ion to electron density is about 5 to 10 and decreases with pressure. The dominant negative ion is O^-, whereas the molecular ions form about 10–20% of the total density. The model in which the previously estimated sticking coefficients and reaction constants are incorporated describes the pressure dependencies of ion densities very well.

The competition between ion-ion recombination (8) and neutral detachment (9,10) explains the observed ion densities, while electronic detachment (11) is of very little importance. At low pressures the O^- balance is governed by dissociative attachment to O_2 (6) and ion-ion recombination (8), which causes its density to increase as the square root of pressure. The densities of the detaching species [O and $O_2(a)$] increase with pressure (see Fig. 13). Therefore neutral detachment (9,10) becomes dominant at pressures above 30 mTorr, resulting in a decrease of the negative ion density. As the detaching species are produced from O_2 (1,3), and lost by diffusion to the wall (22) and/or by flow, their density increases quadratically with pressure, resulting in a p^{-1} dependence of the negative ion density. However, at pressures above 100 mTorr $O_2(a)$ is lost by bulk processes (2,4,7,10,12), so its density becomes linear with pressure. Consequently, the decrease of the negative ion density at higher pressures is less pronounced.

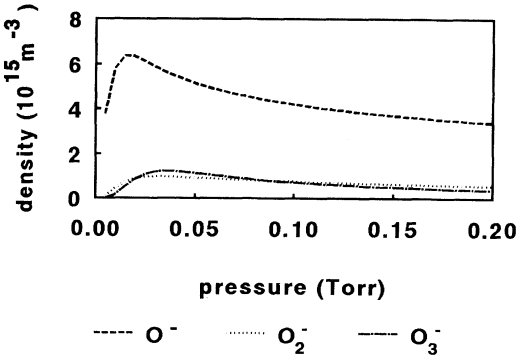

FIG. 12. The calculated ion densities as a function of pressure at $T_e = 3$ eV, for gas flow 30 SCCM and input power 10 W. The sum of these is the total ion density shown in Fig. 11.

The behavior of O_2^- and O_3^- can be explained in a similar way as has been done for O^-. Since the molecular ions are formed mainly by charge exchange between O^- and $O_2(a)$ or O_3 (12,18) and destroyed again by recombination and detachment, the dependencies of their densities on pressure are similar. The maxima can be shifted towards higher pressures, as can be expected considering the pressure dependencies of $[O_2(a)]$ and $[O_3]$ (Fig. 13). Note that the O_3 density is coupled to the $O_2(a)$ density by associative detachment (10).

The pressure dependence of the negative ion density has been calculated for several electron temperatures and the effect of varying T_e is shown in Fig. 14. It can be seen that the negative ion density is only weakly T_e dependent. At low pressures, where the T_e independent recombination (8) is the major loss process, the ion density depends on T_e as the square root of the attachment constant. The latter is hardly T_e dependent at temperatures close to the attachment threshold (4.5 eV), but decreases for temperatures below 2.5 eV. At high pressures the attachment is balanced by the neutral detachment. Since the production rates of detaching species and dissociative attachment have similar temperature dependencies, these temperature effects cancel and the ion density becomes T_e independent.

In order to satisfy the charge neutrality condition, the positive ion density has to match the (temperature independent) negative charge density, from which the ionization rate can be deduced, as explained in Sec. III. This effective ionization rate as a function of pressure is shown in Fig. 15. Its decrease with increasing pressure should be interpreted as an electron temperature decrease, a common feature of low pressure discharges [23,38]. If this ionization rate is compared with the literature value [39], an effective "ionization temperature" as a function of pressure can be found (Fig. 15). The values are very close

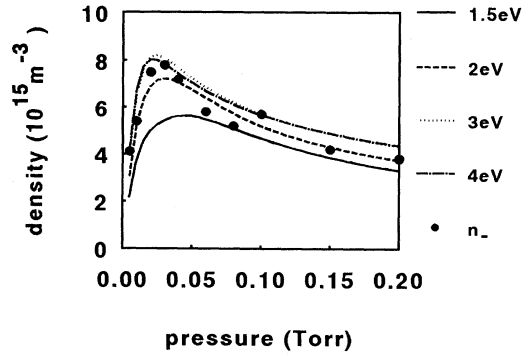

FIG. 14. The calculated total negative ion density as a function of pressure for several electron temperatures. The gas flow is 30 SCCM and the input power is 10 W. The measured data points are added as reference.

to the expected bulk electron temperatures, which suggests that at least for pressures higher than 20 mTorr the electron energy distribution function does not deviate significantly from a Maxwellian. When this pressure dependence of the ionization temperature is used to recalculate the negative ion densities, the resulting curve does not differ appreciably from the one calculated using a constant $T_e = 3$ eV (see Fig. 14). A more strict approach should also account for the non-Maxwellian effects in the EEDF and their pressure dependencies. For example, the rise in the ionization rate at pressures below 20 mTorr can be caused by an increase of the number of electrons in the high energy tail [19,38]. In this case the bulk temperature, which determines the negative ion density, need not vary so much. Concluding, to first order it is justified to use a constant T_e in calculations of the negative ion density, though the ionization temperature shown in Fig. 15 is probably closer to the actual electron temperature.

D. Power dependence

The total negative ion density as a function of rf input power is shown in Fig. 16. Based on the kinetic model

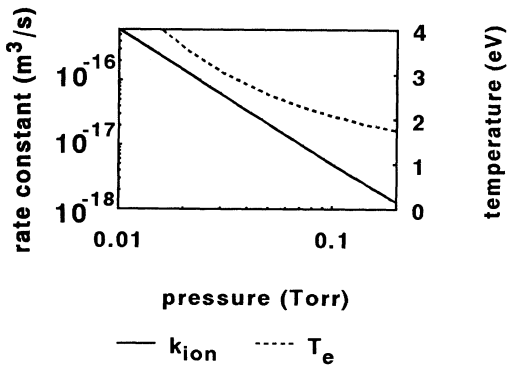

FIG. 15. The ionization rate constant, calculated using Eq. (5), as a function of pressure (solid line) and the corresponding "ionization" temperature of the electrons (dashed line).

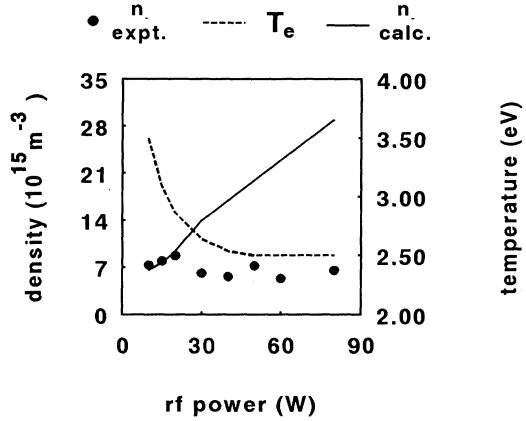

FIG. 16. The total ion density as a function of input power (dots), for 30 SCCM gas flow at 30 mTorr. The solid line represents the calculated density and the dashed line represents the "ionization temperature" of the electrons.

and measurements in other gases [40] it is expected that the negative ion density increases with increasing electron density, but in this case it stays constant in the whole power range, even though the electron density increases by more than a factor of 10 (Fig. 3). At higher rf powers the gas and the electrodes can be significantly heated. This can increase the detachment by $O_2(a)$, according to the mechanism described in Sec. IV B. The influence of the discharge power on surface chemistry has also been reported by Wickramanyaka *et al.* [33]. We note that in our experimental arrangement only the powered electrode is water cooled and thermal contact between the rest of the microwave cavity, the water cooled electrode, and the outer vacuum chamber is poor. A relatively high cavity temperature (60 to 70 °C) was noted when the vacuum system was vented immediately after plasma operation. The temperature increase is expected to cause a significant enhancement of the detaching species density and/or their reactivity at high rf powers so neglecting these effects in the model leads to an overestimation of the calculated negative ion density. The behavior of the measured negative ion density as a function of power gives an independent indication that temperature is important for the negative ion density.

If the measured (constant) ion density is introduced into Eq. 5 it can be seen that the effective ionization constant and consequently the "ionization" temperature has to decrease with increasing rf power. A similar effect has previously been reported in this kind of plasma [23,38].

V. CONCLUSION

The electron and negative ion densities in a low pressure (5–200 mTorr) oxygen rf discharge have been measured. The electron density is about 10^{15} m^{-3} and the negative ion density about five to ten times higher. The dominant negative ion is O^-. The ratio of negative ion to electron density decreases with pressure and rf input power.

The behavior of the negative ion density in this discharge can be explained in terms of plasma and surface reactions. The dominant negative ion, O^-, is produced by dissociative attachment of O_2 and destroyed by ion-ion recombination at low pressures and by neutral detachment at high pressures. The competition between these destruction processes results in a maximum density at about 30 mTorr.

Since negative ion production is only weakly dependent on the electron temperature, the densities can be modeled using a constant temperature for the range of plasma conditions investigated. However, the negative charge density must always balance the positive ion density, which is extremely electron temperature dependent through the ionization rate. The ionization rate, determined from the total negative charge density, is used to calculate the electron ionization temperature and its dependence on plasma conditions. This yields a temperature between 2 and 4 eV, decreasing with pressure and rf power. These values and trends agree well with those expected for the bulk electron temperature.

It has been shown that neutral gas chemistry has a strong influence on the negative ion density and that experimental dependencies upon plasma parameters in combination with modeling help to decide on the relative importance of various processes. The surface chemistry appears to be strongly related to the wall conditions; further study of wall processes and their dependencies upon the condition of the wall material is needed for a complete description of the discharge chemistry. The present work suggests that the gas and the wall temperatures are important and control of these parameters in experiments appears to be essential if the remaining uncertainties are to be resolved. On a more positive note, the results also suggest that the discharge chemistry, and in particular the negative ion density, can be directly influenced simply by controling these temperatures.

APPENDIX

Heterogeneous processes can have a significant influence on the discharge chemistry and therefore they have to be treated in kinetic models. In zero-dimensional models this is a problem since all processes are assumed to be homogeneous. It is then necessary to introduce a homogeneous production or loss frequency to account for heterogeneous processes.

For diffusion problems having the general form

$$(\text{production} - \text{destruction}) + D\nabla^2 n(x) = \frac{\partial n(x)}{\partial t}, \quad \text{(A1)}$$

an effective diffusion frequency can be estimated by D/Λ_{eff}^2, if the effective gradient length Λ_{eff} is found. The value of this gradient length depends on the geometry of the reactor, the form of the production and destruction terms, and the boundary conditions (e.g., sticking coefficients). Chantry [41] calculated Λ_{eff} for partially absorbing walls in several geometries by solving the time dependent diffusion equation without production and destruction terms. This solution is also valid if these terms are linear in the density $n(x)$ (e.g., electron impact ionization in the balance equation for electrons). However, we need an effective gradient length to describe the losses of atomic oxygen at the wall in the stationary state ($\partial n/\partial t = 0$). In this case the production is constant [not proportional to $n(x)$] in the plasma glow and equal to zero in the sheath. Bulk destruction of atomic oxygen can also be neglected. Therefore the balance can be written

$$P + D\nabla^2 n(x) = 0, \quad \text{(A2)}$$

with the production term for oxygen given by $P = 2\{k_1[O_2]n_e + k_2[O_2(a)]n_e\}$ in our model. As the height of the plasma glow is much smaller than its radius, we can neglect radial diffusion. The production takes place only in the plasma glow (thickness H_g) and the solution and its derivative are continuous at the edge of the glow. For a partially absorbing wall, with a sticking coefficient γ, the boundary condition at the wall is found by considering the particle in and outflux for a small volume at the wall. The number of particles per unit area and time (Φ_x) moving in direction x is given by

$$\Phi_x = \frac{1}{4}nv - \frac{1}{6}\lambda v\frac{dn}{dx}, \quad \text{(A3)}$$

where the mean free path λ is related to the thermal velocity v by $\lambda = 3D/v$. The number of particles moving in the opposite direction (Φ_{-x}) is

$$\Phi_{-x} = \frac{1}{4}nv + \frac{1}{6}\lambda v\frac{dn}{dx}. \quad \text{(A4)}$$

In a stationary state the net flux of particles to the volume at the wall ($\Phi_x - \Phi_{-x}$) from the plasma has to equal the net flux towards the wall ($\gamma\Phi_x$). This yields the boundary condition

$$\left.\frac{dn}{dx}\right|_{\text{wall}} = -\frac{1}{\xi}n_w, \quad \text{(A5)}$$

where n_w is the density at the wall and

$$\xi = \frac{2\lambda(2-\gamma)}{3\gamma}. \quad \text{(A6)}$$

From the above, the densities in the glow and the sheaths are
glow:

$$n(x) = \frac{P}{2D}\left[\frac{H_g}{2}\left(2\xi + H - \frac{H_g}{2}\right) - x^2\right], \quad \text{(A7)}$$

sheath:

$$n(x) = \frac{PH_g}{2D}\left(\xi + \frac{H}{2} \pm x\right) \quad \text{(A8)}$$

and the average density in the plasma glow is

$$\langle n_g \rangle = \frac{P}{D}\frac{H_g}{4}\left(2\xi + H - \frac{2}{3}H_g\right) \qquad \text{(A9)}$$
$$= \frac{P}{D}\Lambda_{\text{eff}}^2.$$

Neglecting the sheath leads to

$$\Lambda_{\text{eff}}^2 = \frac{H^2}{12} + \frac{\xi H}{2}, \qquad \text{(A10)}$$

where the first term represents the usual gradient length obtained assuming that the density at the wall equals zero. This assumption is valid for strongly absorbing walls and high pressures. The second term becomes important when $\lambda \sim \gamma H$, which occurs for low pressures and/or low sticking coefficients.

The same formalism can be used to estimate the effective gradient length for positive ions in the electronegative plasma when their production is also homogeneous in the plasma glow. Assuming that the positive ion density drops to zero near the edge of the sheath results in an approximate gradient length of $H_g/\sqrt{12}$.

[1] M. Saitoh, K. Kanazawa, T. Momose, H. Ishimaru, N. Ota, and J. Uramoto, J. Vac. Sci. Technol. **11A**, 2518 (1993).

[2] S. Taylor, J.F. Zhang, and W. Ecclestone, Semicond. Sci. Technol. **8**, 1426 (1993).

[3] Hong-Xing You, N.M.D. Brown, and K.F. Al-Assadi, Surf. Sci. **284**, 263 (1993).

[4] T. Oda, T. Takahashi, H. Nakano, and S. Masuda, IEEE Trans. Ind. Appl. **29**, 787 (1993).

[5] R.A. Gottscho and T.A. Miller, Pure Appl. Chem. **56**, 189 (1984).

[6] R.W. McCullough, J. Geddes, A. Donnely, M. Liehr, M.P. Hughes, and H.B. Gilbody, Meas. Sci. Technol. **4**, 79 (1993).

[7] H. Amemiya, K. Ogawa, T. Suzuki, and M. Endou, J. Phys. D **26**, 2174 (1993).

[8] G. Gousset, C.M. Ferreira, M. Pinheiro, P.A. Sa, M. Touzeau, M. Vialle, and J. Loureiro, J. Phys. D **24**, 290, (1991).

[9] A.T. Bell, Ind. Eng. Chem. Fundam. **10**, 373 (1971).

[10] I.A. Kossyi, A.Yu. Kostinsky, A.A. Matveyev, and V.P. Silakov, Plasma Sources Sci. Technol. **1**, 207 (1992).

[11] K. Tachibana, in *The 11th International Symposium on Plasma Chemistry, Symposium Proceedings*, edited by J. E. Harry (International Organizing Committee of the International Symposium on Plasma Chemistry 11, Loughborough, U.K., 1993), Vol. 1, p. 344.

[12] H. Amemiya and T. Suzuki, Plasma Sources Sci. Technol. **1**, 94 (1992).

[13] H. Kersten and J.F. Behnke, in *the 11th International Symposium on Plasma Chemistry* (Ref. [11]), Vol. 3, p. 656.

[14] N. Yasuda, H. Amemiya, and M. Endo, in *Proceedings of the 2nd International Conference on Reactive Plasmas and 11th Symposium on Plasma Processing*, edited by T. Goto (Organizing Committee of ICRP-2/SPP-11, Yokohama, Japan, 1994), p. 613.

[15] T. Suzuki and T. Kasuya, Phys. Rev. A **36**, 2129 (1987).

[16] J.L. Jauberteau, G.J. Meeusen, M. Haverlag, G.M.W. Kroesen, and F.J. De Hoog, J. Phys. D **24**, 261 (1991).

[17] M. Endo, S. Kishimoto, A. Kono, and T. Goto, in *Proceedings of the 2nd International Conference on Reactive Plasmas and the 11th Symposium on Plasma Processing* (Ref. [14]), p. 605.

[18] J.D.P. Passchier and W.J. Goedheer, J. Appl. Phys. **73**, 1073 (1993).

[19] A.J. Lichtenberg, V. Vahedi, M.A. Lieberman, and T. Rognlien, J. Appl. Phys. **75**, 2339 (1994).

[20] M. Haverlag, Ph.D. thesis, Eindhoven University of Technology, 1991.

[21] D.M. Neumark, K.R. Lykke, T. Andersen, and W.C. Lineberger, Phys. Rev A **32**, 1890 (1985).

[22] P.S. Drzaic, J. Marks, and J.I. Brauman, in *Gas Phase Ion Chemistry*, edited by M.T. Bowers (Academic Press, Orlando, 1984), Vol. 3, p. 167.

[23] T. Kaneda, T. Kubota, M. Ohuchi, and Jen-Shih Chang, J. Phys. D **23**, 1642 (1990).

[24] M. Mizumura, S. Uotsu, S. Matsumura, and S. Teii, J. Phys. D **25**, 1744 (1992).

[25] R.J.M.M. Snijkers, M.J.M. van Sambeek, G.M.W. Kroesen, and F. J. de Hoog, Appl. Phys. Lett. **63**, 308 (1993).

[26] L.G. Christophorou, *Electron-Molecule Interactions and Their Applications* (Academic Press, New York, 1984).

[27] V.G. Samoilovich, M.P. Popovich, Yu.M. Emelyanov, and Yu.V. Filippov, Russ. J. Phys. Chem. **40**, 287 (1966).

[28] B.M. Smirnov, *Negative Ions* (McGraw-Hill, New York, 1982).

[29] G. Fournier, in *Cinétique de l'oxygène en milieu plasma* in *Ecole d'été réactivité dans les plasmas. Applications aux lasers et aux traitement de surfaces*, edited by A.-M. Pointu and A. Ricard (Les Editions de Physique, Les Ulis, France, 1983).

[30] B. Peart, R.A. Forrest, and K. Dolder, J. Phys. B **12**, 2735 (1979).

[31] J.P. Booth and N. Sadeghi, J. Appl. Phys. **70**, 611 (1991).

[32] R.L. Sharpless and T.G. Slanger, J. Chem. Phys. **91**, 7947 (1989).

[33] S. Wickramanayaka, N. Hosokawa, and Y. Hatanaka, Jpn. J. Appl. Phys. **30**, 2897 (1991).

[34] B. Jackson and M. Persson, J. Chem. Phys. **96**, 2378 (1992).

[35] L.E. Khvorostovskaya and V.A. Yankovsky, Contrib. Plasma Phys. **31**, 71 (1991).

[36] E. Stoffels, W.W. Stoffels, L.C.T. Verhamme, E. Van Wieringen, G.M.W. Kroesen, and F.J. De Hoog, Europhys. Conf. Abstracts **16F**, 455 (1992).

[37] R.L. Sharpless, L.E. Jusinski, and T.G. Slanger, J. Chem. Phys. **91**, 7936 (1989).

[38] V.A. Godyak, R.B. Piejak, and B.M. Alexandrovich, Plasma Sources Sci. Technol. **1**, 36 (1992).

[39] T.D. Märk, J. Chem. Phys. **63**, 3731 (1975).

[40] E. Stoffels, W.W. Stoffels, A.J. Snoeijer, E.W.M. Knols, G.M.W. Kroesen, and F.J. De Hoog, in *Proceedings II, XXI International Conference on Phenomena in Ionized Gases*, edited by G. Ecker, U. Arendt, and J. Böseler (Arbeits Gemeinschaft, Plasma Physik, Bochum, Germany, 1993), p. 247.

[41] P.J. Chantry, J. Appl. Phys. **62**, 1141 (1987).